ISSCR

Dissecting signaling hierarchies in the patterning of the mouse primitive streak using micropatterned EpiLC colonies

Jean-Louis Plouhinec,[1,4] Gaël Simon,[1,2,4] Mathieu Vieira,[2] Jérôme Collignon,[2,*] and Benoit Sorre[1,3,*]

[1]Université Paris Cité, CNRS, Laboratoire Matière et Systèmes Complexes, 75013 Paris, France
[2]Université Paris Cité, CNRS, Institut Jacques Monod, 75013 Paris, France
[3]Institut Curie, Université PSL, Sorbonne Université, CNRS UMR168, Laboratoire Physico Chimie Curie, 75005 Paris, France
[4]These authors contributed equally
*Correspondence: jerome.collignon@ijm.fr (J.C.), benoit.sorre@curie.fr (B.S.)
https://doi.org/10.1016/j.stemcr.2022.05.009

SUMMARY

Embryo studies have established that the patterning of the mouse gastrula depends on a regulatory network in which the WNT, BMP, and NODAL signaling pathways cooperate, but aspects of their respective contributions remain unclear. Studying their impact on the spatial organization and developmental trajectories of micropatterned epiblast-like cell (EpiLC) colonies, we show that NODAL is required prior to BMP action to establish the mesoderm and endoderm lineages. The presence of BMP then forces NODAL and WNT to support the formation of posterior primitive streak (PS) derivatives, while its absence allows them to promote that of anterior PS derivatives. Also, a *Nodal* mutation elicits more severe patterning defects *in vitro* than in the embryo, suggesting that ligands of extra-embryonic origin can rescue them. These results support the implication of a combinatorial process in PS patterning and illustrate how the study of micropatterned EpiLC colonies can complement that of embryos.

INTRODUCTION

In the mouse embryo, the patterning of the pluripotent epiblast culminates at embryonic day (E) 6.5 with the formation of the primitive streak (PS), where posterior epiblast cells undergo the epithelial-mesenchymal transition (EMT) associated with the adoption of mesendodermal cell identities. The PS itself is patterned, as cells that emerge at different levels of the PS have distinct fates: extra-embryonic mesoderm and embryonic mesoderm when emerging posteriorly and axial mesoderm and definitive endoderm when emerging anteriorly (Kinder et al., 1999).

The signaling molecules WNT3, bone morphogenic protein 4 (BMP4), and NODAL, are essential to form the PS, a loss of function of any one of them being sufficient to cause its absence (Brennan et al., 2001; Conlon et al., 1994; Liu et al., 1999; Winnier et al., 1995; Zhou et al., 1993). Analyses of mutant phenotypes, as well as studies performed in other model vertebrates, have shown that BMP4 promotes posterior mesoderm differentiation and counteracts the effect of NODAL, which acts in concert with the WNT/β-catenin pathway to promote anterior mesendodermal fates (Ben-Haim et al., 2006; Conlon et al., 1994; Harland, 1994; Vincent et al., 2003; Zorn et al., 1999). These studies led to a model of the mouse PS, where its anterior-posterior (A/P) patterning is governed by opposing gradients of NODAL and BMP4 signaling activities (Morgani and Hadjantonakis, 2020).

Although cell-fate allocation in the mouse PS appears to depend on the level of NODAL signaling, there is little evidence of a NODAL signaling gradient along the A/P axis of the PS (Norris et al., 2002; Peng et al., 2016). Investigating this issue in the developing mouse embryo is challenging. One difficulty stems from the demonstrated interdependence of *Wnt3*, *Bmp4*, and *Nodal* and another from their earlier roles in embryo patterning (Camacho-Aguilar and Warmflash, 2020; Morgani and Hadjantonakis, 2020).

An *in vitro* approach, allowing better control of the conditions under which epiblast patterning takes place, now provides an alternative to conduct these investigations. Human embryonic stem cells (hESCs), cultured as a monolayer on embryo-size circular adhesive micropatterns, self-organize when exposed to BMP4 and give rise to the three embryonic germ layers, arranged in concentric rings, in an ordered and reproducible sequence, forming so-called human 2D-gastruloids (h2Dgas) (Warmflash et al., 2014). A recent study showed that mouse epiblast-like cells (EpiLCs), pluripotent cells derived from mouse ESCs (mESCs), can similarly be used to generate m2Dgas (Morgani et al., 2018).

Here we describe our use of m2Dgas to study *in vitro* the role of WNT3, BMP4, and NODAL during gastrulation. Consistent with previous studies (Morgani and Hadjantonakis, 2021; Morgani et al., 2018), our results validate the ability of m2Dgas to recapitulate key aspects of gastrulation when stimulated by BMP or WNT signals. The effects of two *Nodal* mutations on m2Dgas patterning then provide new insights into the role of *Nodal* in cell-fate specification during gastrulation.

RESULTS

BMP4 triggers EpiLC colony patterning

Unlike mESCs, EpiLCs have the ability to respond to germ cell and PS-inductive cues and are, therefore, considered to

A

Seeding on μ-patterns

| 2i+LIF | ACTIVIN+FGF2 | ACTIVIN+FGF2+BMP4 (BAF) | Ø |

-48h   EpiLC induction   0h   EpiLC differentiation   48h   72h

B   EpiLC (BMP4+Activin+FGF2)

24h   48h   72h

POU5F1   NANOG   BRACHYURY   SOX17   FOXA2   CDX2

n/a

C

t = 24h   t = 48h   t = 72h

mean fluo (A.U.)

Position from colony center (μm)
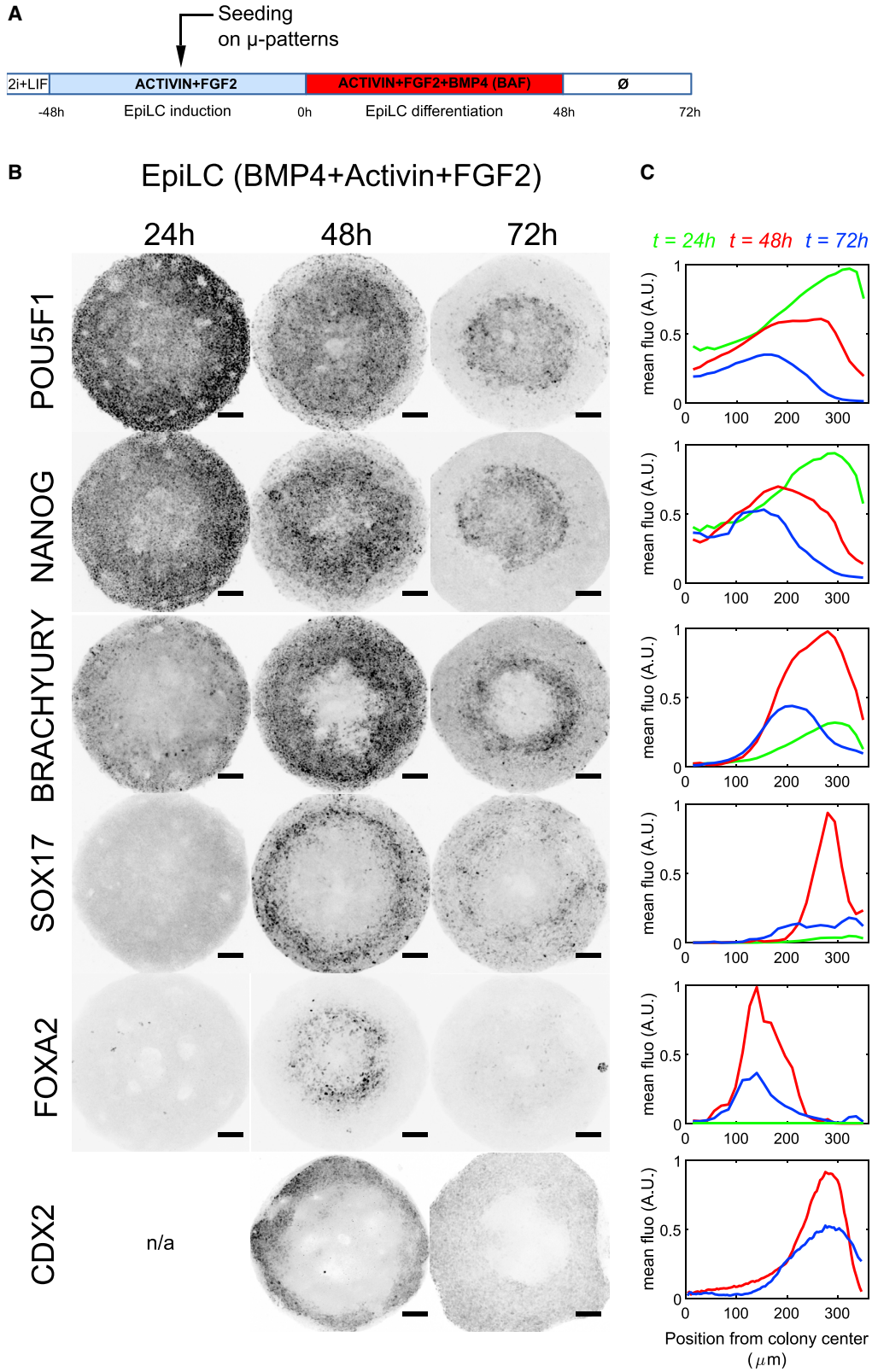
(legend on next page)

be in a state of formative pluripotency (Hayashi et al., 2011; Kinoshita et al., 2021), which is well suited to recapitulate epiblast patterning *in vitro*.

To initiate their conversion into EpiLCs, mESCs were seeded on fibronectin-coated Petri dishes in N2B27 + ACTIVIN + FGF medium (t = −48 h, Figure 1A). After 24 h, they were transferred on adhesive micropatterned substrates (700μm in diameter) obtained by microcontact printing of fibronectin onto PDMS-coated glass slides and left for another 24 h. This two-step protocol ensures homogeneous seeding of the adhesive micropatterns, which is key to patterning reproducibility. At 48 h after the start of the culture (t = 0, Figure 1A), cells in the colonies showed an expression profile consistent with the acquisition of an EpiLC identity (Figures S1A and S1B) (Hayashi et al., 2011). BMP4 was then added to the EpiLC differentiation medium (t = 0, 50 ng/mL) to trigger PS formation. The differentiation of the colonies was characterized by immunofluorescence (IF) after 24, 48, and 72 h of culture.

Pluripotency in the post-implantation embryo tracks the expression of Pou5f1 (OCT4), which is initially present throughout the epiblast but is lost from mesendodermal cells as they emerge from the PS (Osorno et al., 2012). NANOG expression at these stages begins in the proximal epiblast but rapidly expands to the posterior epiblast, where it persists on either side of the emerging PS. At 24 h after the addition of BMP4, these two factors were expressed throughout the colonies, with levels increasing from the colony center to its outer region (Figure 1B). IF at 48 and 72 h showed that the expression of OCT4 and NANOG then progressively decreased and was restricted to the center of the colonies, suggesting that epiblast cells persisted there.

The pan-mesodermal marker Brachyury (BRA, also known as T), which begins to be expressed in the posterior epiblast at E6.0–E6.25, shortly before PS formation (Perea-Gomez et al., 2004; Rivera-Pérez and Magnuson, 2005), was detected in the colonies 24 h after induction, in a large outer ring of cells (Figure 1B). This expression strengthened after 48 h and moved inward to a more central position at 72 h. SOX17 expression was detected in a thin ring of cells within the BRA expression domain at 48 h. Both factors are expressed in the embryo in extra-embryonic mesoderm cells, which emerge from the posterior PS, and in definitive endoderm (DE) cells emerging from the anterior PS (Burtscher

and Lickert, 2009). To determine which of these two possibilities fits the pattern we obtained, we examined CDX2, which is co-expressed with SOX17 in some posterior mesoderm derivatives, and FOXA2, which is present in posterior epiblast, anterior PS, and axial mesodermal cells and co-expressed with SOX17 in DE cells (Burtscher and Lickert, 2009). CDX2 was detected at the colony periphery at 48 and 72 h. In contrast, FOXA2 expression was detected in a ring of cells closer to the center, overlapping with NANOG-positive cells but not SOX17-positive cells. FOXA2 expression in BMP4-stimulated colonies is thus associated with a posterior epiblast identity, whereas SOX17 expression is associated with an extra-embryonic mesoderm identity. The fact that SOX17 and FOXA2 were not co-expressed and that FOXA2 expression was no longer detected 72 h after BMP4 addition strongly suggests that DE and axial mesoderm do not form on BMP4-stimulated colonies.

These results, in agreement with a previous report (Morgani et al., 2018), thus showed that when exposed to BMP4, EpiLC colonies form a specific differentiation pattern, with a ring of mesoderm surrounding a core of epiblast, both biased toward posterior identities, as embryological studies led us to expect (Kinder et al., 1999).

Sustained BMP exposure prevents the establishment of distal cell identities

Post-implantation epiblast cells express NODAL and fibroblast growth factor (FGF), but the BMP4 and WNT3 they detect are initially produced by adjacent extra-embryonic cells (Rivera-Pérez and Magnuson, 2005; Winnier et al., 1995). Only once patterning has begun do proximal and posterior embryonic cells start to express *Bmp4* and *Wnt3* themselves. In line with these facts, EpiLCs express *Nodal*, *Fgf4*, *Fgf5*, and *Fgf15*, but none of the relevant *Bmp* or *Wnt* genes (Du et al., 2018). This suggests that the addition of recombinant WNT or BMP is required to initiate EpiLC colony patterning, whereas the addition of recombinant NODAL and FGF is not, as their endogenous production may suffice.

To test these hypotheses, and to investigate the respective roles of these morphogens, we compared the developmental trajectories of colonies stimulated with different combinations of ACTIVIN(A, a proxy for NODAL), BMP4 (B), FGF2 (F), and WNT3A (W, a proxy for WNT3). As previously reported, the absence of ACTIVIN had little impact

Figure 1. BMP4-induced differentiation of m2Dgas

(A) Protocol to generate differentiated EpiLC colonies on micropatterns. Ø indicates that no morphogens were added to the culture medium.

(B) Maximum intensity projections of immunostained m2Dgas (700 μm) 1, 2, or 3 days after the start of BMP4 stimulation. For clarity, contrast is inverted. Similar results were obtained in at least two independent experiments.

(C) Fluorescence intensity levels normalized to the maximum value obtained and averaged along the colony radii at t = 24, 48, and 72 h. POU5F1 (n = 18, 24, and 24), NANOG (n = 3, 3, and 3), SOX2 (n = 3, 3, and 3), Brachyury (n = 15, 18, and 18), SOX17 (n = 3, 6, and 6), FOXA2 (n = 3, 3, and 3), and CDX2 (n = 3 and 3). Scale bar, 100μm.
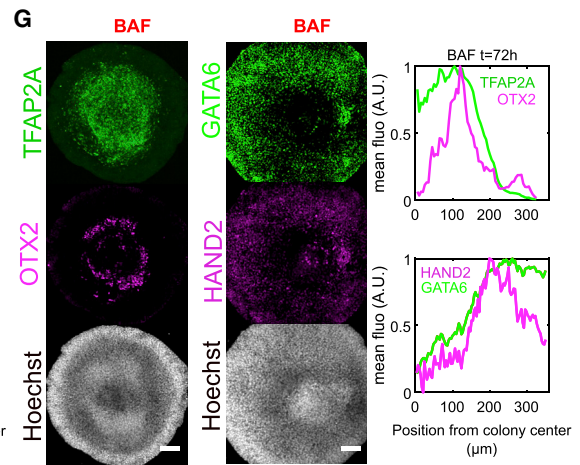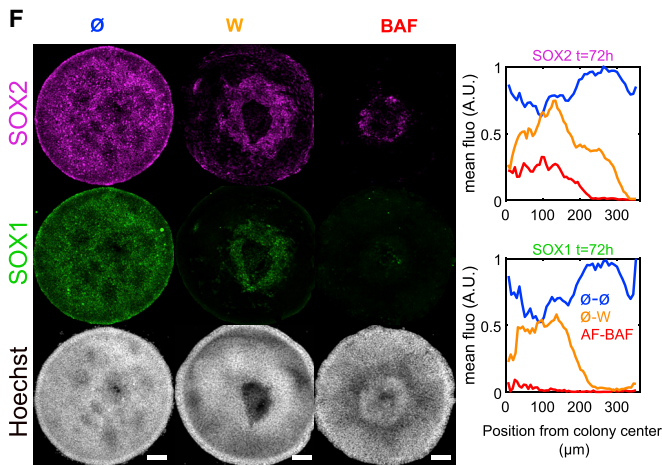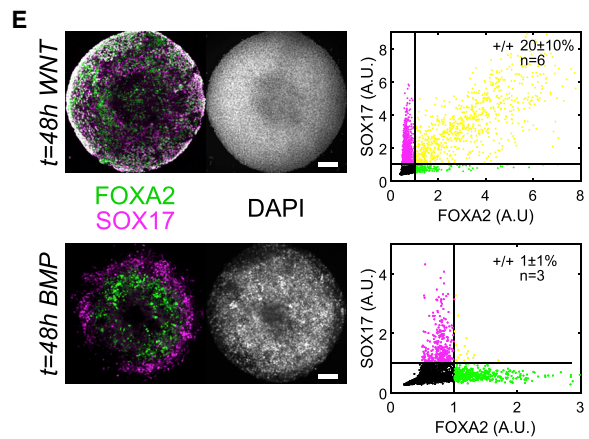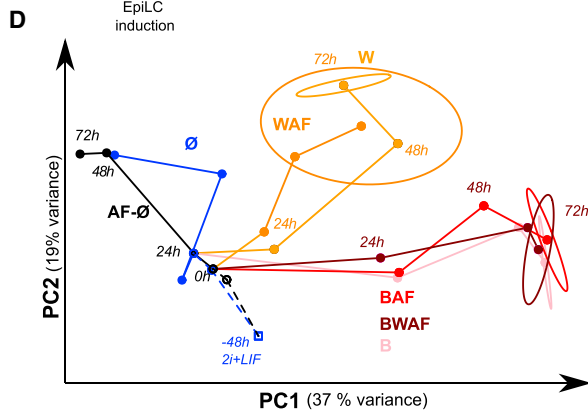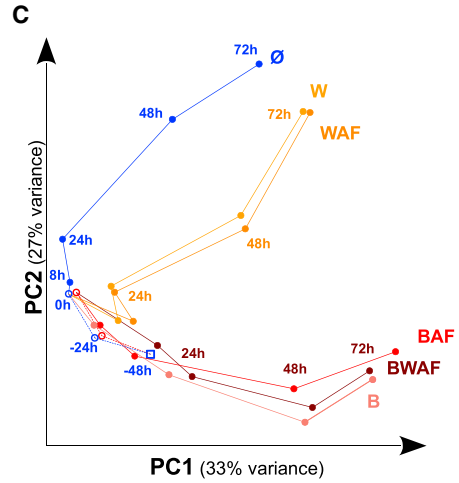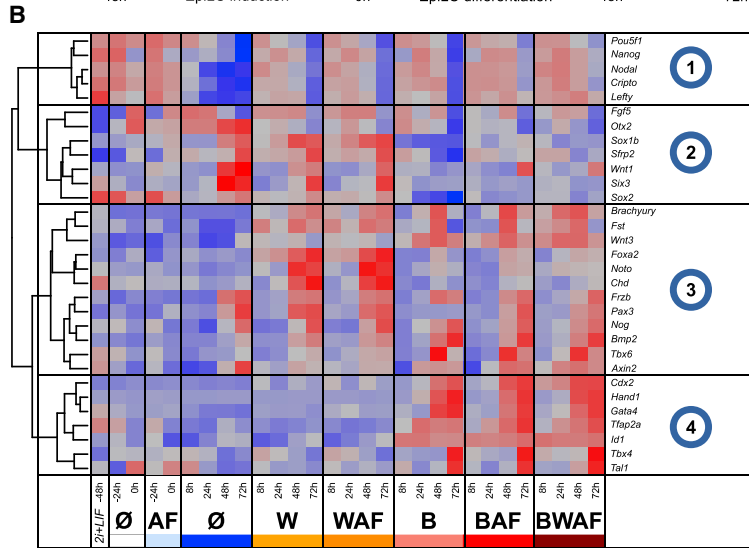
(legend on next page)

on the conversion of ESCs into EpiLCs, presumably because of endogenous NODAL production (Figure S1B) (Buecker et al., 2014). Endogenous production of FGF probably explains that its addition was likewise unnecessary (Figure S1B). Some EpiLC colonies obtained without the addition of AF were thus left to differentiate on their own (∅) or were treated for 48 h with B or W. Other EpiLC colonies, obtained as before in the presence of AF, were then treated for 48 h with BAF, WAF, or BWAF. All colonies were then left to differentiate autonomously for a further 24 h, without morphogen added, as by that stage they themselves produce the signaling molecules necessary to sustain their differentiation.

IF detection of cell-type specific markers has so far been the main approach used to characterize the differentiation of 2Dgas (Deglincerti et al., 2016; Etoc et al., 2016; Martyn et al., 2019; Morgani et al., 2018; Warmflash et al., 2014). It provides a spatial record of the result but the number of markers that can be monitored at the same time is limited and the availability of antibodies constrains their choice. Furthermore, the resulting data are not easily exploitable for principal-component analysis (PCA), a statistical tool commonly used to distinguish cell identities based on gene expression. The quantification of gene expression in pooled colonies thus emerged as a complementary approach to track and compare developmental trajectories.

The first experiment was thus performed as follows. We collected samples at t = −48, −24, 0, 8, 24, 48, and 72 h and quantified by RT-qPCR the expression of 31 markers, specifically selected to follow post-implantation embryo patterning (Peng et al., 2016; Pijuan-Sala et al., 2019) (Table S1). They included known targets of signaling pathways, such as *Id1* (BMP target), *Axin2* (WNT/β-catenin target), and *Lefty2* (ACTIVIN/NODAL target); genes encoding secreted antagonists, such as *Noggin*, *Chordin*, and *Lefty2*; and several lineage markers, such as *Noto* (axial mesoderm) and *Sox1b* (neurectoderm). The genes were clustered according to the similarity of their expression dynamics (Figures 2A and 2B): cluster 1 markers were found to track the disappearance of the epiblast identity (in all colonies regardless of the treatment); cluster 2 markers, the emergence of an ectodermal/neural identity (in ∅, W, and WAF colonies); cluster 3 markers, the emergence of both anterior (in W and WAF colonies) and posterior (in B, BAF, and BWAF colonies) embryonic derivatives of the PS; and cluster 4 markers, the emergence of extra-embryonic derivatives of the posterior PS (in B, BAF, and BWAF colonies). To visualize the developmental trajectories, we projected the gene expression data in the plane formed by the first two principal components of the dataset, which together capture about 60% of the variance (Figure 2B). This analysis suggested that the different treatments led to only three types of trajectories: toward neurectoderm (∅); toward distal identities (W and WAF); and toward proximal identities (any treatment containing B).

A second experiment, analyzed using a slightly different set of markers, gave similar results (Figures S2A and S2B). To assess the statistical relevance of the data and define averaged trajectories, a third replicate was generated. To prevent batch effects and be able to normalize gene expression to a common reference for all replicates, gene expression levels must be quantified in the same RT-qPCR experiment. To carry out the experiment efficiently, we selected the two or three genes in each cluster that in our previous analysis commanded the highest share of the variance, measured their expression in all three replicates, and performed a PCA on the resulting dataset (Figure S2C). The mean trajectories thus obtained confirmed that all BMP4-stimulated samples (B, BAF, and BWAF) followed a similar path and reached endpoints that were not statistically distinguishable, as defined by the overlap of their respective 95% confidence ellipses (Figure 2D). The results also showed that AF did not alter the developmental trajectory of W-induced colonies either, even though it had the potential to increase the activity of the ACTIVIN/NODAL and FGF signaling pathways beyond what endogenous ligands normally

Figure 2. BMP prevents the establishment of distal cell identities

(A) Timelines of the different protocols whose effects on EpiLC colony differentiation were compared. Ø, no morphogens; A, ACTIVIN, 20 ng/mL; B, BMP4, 50 ng/mL; F, FGF2, 12 ng/mL; W, WNT3A, 200 ng/mL.

(B) Gene expression matrix obtained via RT-qPCR of pooled colonies at similar time points for each of the six treatments shown in (A). The comparison of gene expression dynamics led to the grouping of markers into four distinct clusters (see main text for details).

(C) Projection of the RT-qPCR data shown in (B) in the space defined by the first two principal components (PCs) of the dataset allows a comparison of the developmental trajectories obtained for each treatment.

(D) Average developmental trajectories obtained from three independent experiments using a selection of 12 markers. The statistical proximity of the endpoints is defined by the overlap of their 95% confidence ellipses.

(E) (Left) Maximum intensity projections (MIPs) of representative immunostained m2Dgas (700 um) 48 h after the start of WNT3A (top) or BMP4 (bottom) stimulation. (Right) Quantification of FOXA2 and SOX17 expression in several m2Dgas; each dot represents a single cell. The upper right quadrant shows the ratio of double-positive cells (yellow).

(F and G) MIPs of representative m2Dgas immunostained 72 h after the start of stimulation with the treatments indicated, and corresponding average fluorescence intensity radial profiles (n = 4). Scale bar, 100μm.
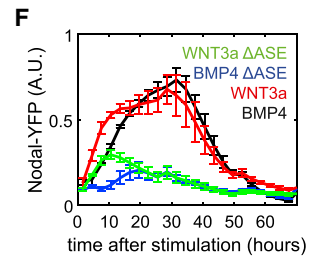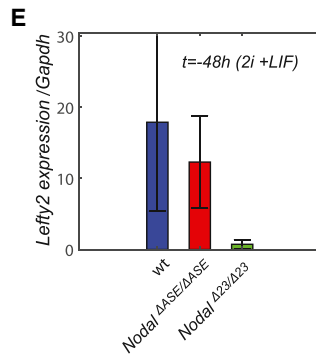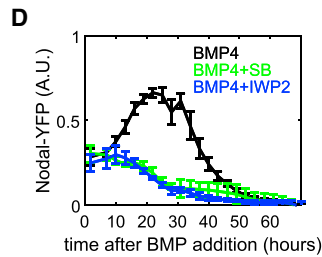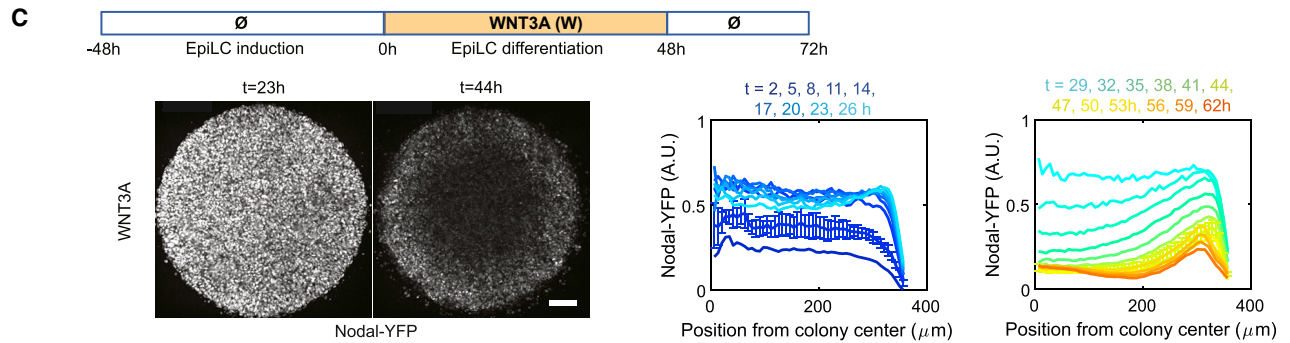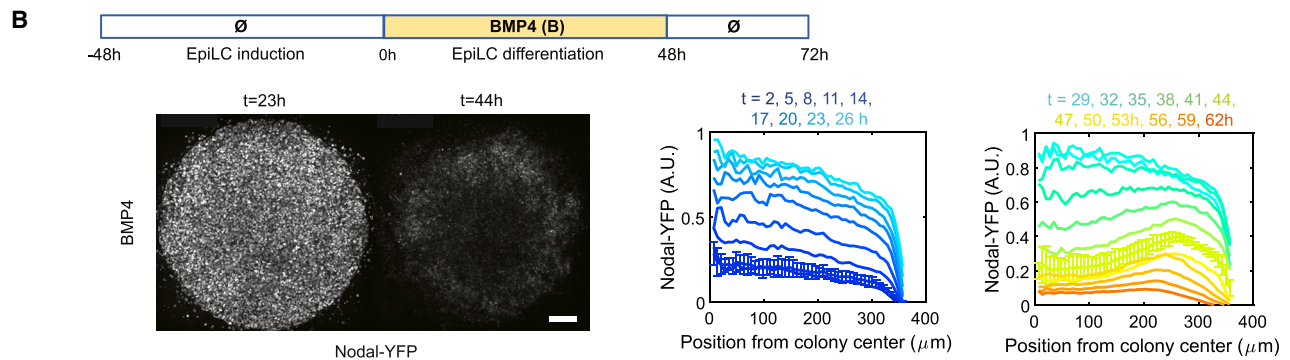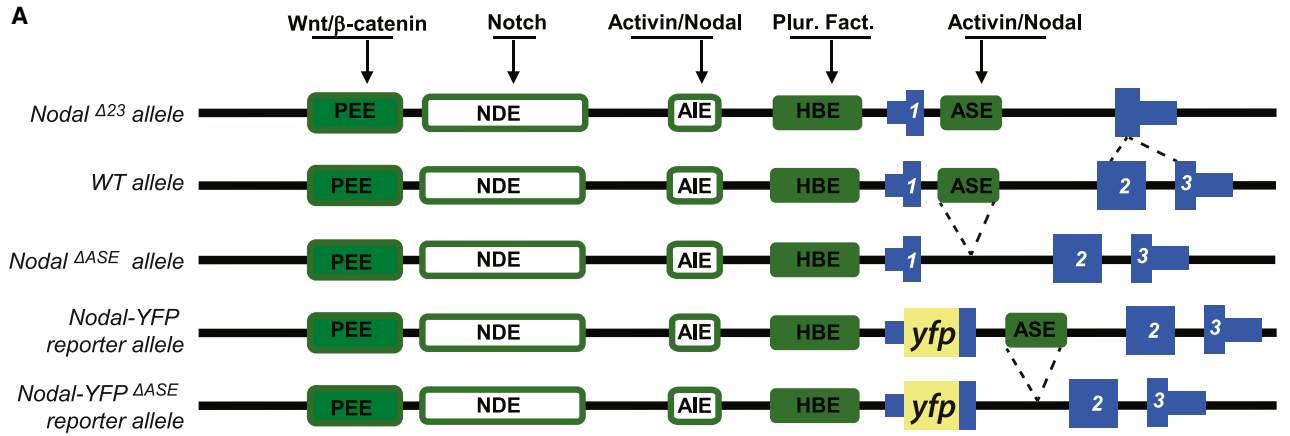
(legend on next page)

achieve. However, in the absence of WNT or BMP stimulation, as in the ∅ condition, *Nodal* expression was not maintained in EpiLCs, confirming the essential requirement for these signaling activities upstream of *Nodal*, and the colonies differentiated toward anterior ectodermal and neural identities, exhibiting a complete absence of PS and PS derivative markers.

Immunostaining of the colonies obtained in these experiments confirmed the cell identities formed in response to each treatment and revealed their position. In W-treated colonies, co-expression of FOXA2 and SOX17 identified the presence of DE cells (Figure 2E). The fact that the expression of these two markers remained separate in BMP-treated colonies marked, as before, the formation of posterior and extra-embryonic mesodermal derivatives. The homogeneous expression of SOX1 and SOX2 in untreated (∅) colonies confirmed they formed neurectoderm (Figure 2F). In W-treated colonies, this neurectodermal identity was restricted to the center, whereas it was completely absent in BAF-treated colonies. Staining for OTX2, TFAP2A, GATA6, and HAND2 nevertheless confirmed the presence of an inner core of non-neural ectoderm and an outer ring of posterior mesoderm in BAF-treated colonies (Figure 2G).

These analyses show that, unlike BMP4, the W and WAF treatments promote the formation of anterior epiblast and anterior PS derivatives. The addition of BMP4, however, largely prevented the establishment of these identities, while promoting proximal fates. Interestingly, this did not appear to involve blocking WNT or ACTIVIN/NODAL signaling because the expression of *Wnt3* and *Nodal* as well as that of their respective feedback inhibitors, *Axin2* and *Lefty2*, was more strongly induced in the presence of BMP4. We focused our attention on the role of endogenously produced NODAL.

m2Dgas recapitulate *Nodal* regulation in the epiblast

First, using a $Nodal^{+/YFP}$ reporter line—where one copy of the gene expresses yellow fluorescent protein (YFP) instead of the ligand (Figure 3A [Papanayotou et al., 2014])—we recorded the spatiotemporal dynamics of *Nodal* expression in differentiating colonies by time-lapse imaging. Stimulation with B or W both resulted within a few hours in a strong and homogeneous induction of *Nodal* expression in the entire colony (Figures 3B and 3C). This expression peaked at t = 24 h and then decreased, disappearing more rapidly in the center of the colony than in its periphery (Figures 3B and 3C), Video S1. The ring of cells where *Nodal* expression persisted longest was also positive for phospho-SMAD2 (pSMAD2) and was part of the BRA expression domain (Figures 1B, 3B, 3C, S3A, and S3B). This dynamic is reminiscent of the progressive restriction of *Nodal* expression to the posterior epiblast and the PS in gastrula stage embryos (Collignon et al., 1996).

Nodal expression in the post-implantation epiblast depends firstly on its own signaling pathway and secondly on a signaling cascade where BMP4 activates *Wnt3* and WNT3 increases *Nodal* expression (Ben-Haim et al., 2006; Norris et al., 2002). We found that inhibiting ACTIVIN/NODAL signaling with SB431542 or WNT secretion with IWP2 similarly impaired the induction of *Nodal* expression in B-stimulated colonies, confirming that this expression is, like in the embryo, dependent on both signaling pathways (Figure 3D). Together with our previous observation that *Wnt3* expression is most induced in B-stimulated colonies (Figure 2B), these results are consistent with m2Dgas adequately replicating the roles played by BMP4 and WNT3 upstream of *Nodal* expression in the post-implantation embryo.

The effect of *Nodal* on its own expression is mediated by the asymmetric enhancer (ASE) (Figure 3A (Norris et al., 2002; Yamamoto et al., 2001), whereas the effect of WNT3 is mediated by the proximal epiblast enhancer (PEE) (Ben-Haim et al., 2006). In nascent epiblast, *Nodal* expression is initially under the control of the highly bound element (HBE) enhancer, but ASE becomes the predominant *Nodal* enhancer during epiblast maturation

Figure 3. Key aspects of *Nodal* regulation are recapitulated during m2Dgas patterning

(A) Schematics of the *Nodal* alleles used in this study. Exons are in blue, enhancers in green. White-filled enhancers are inactive at gastrulation stages. Genotypes of the cell lines used below: WT, $Nodal^{+/+}$; Nodal-YFP, $Nodal^{+/yfp}$; ΔASE-Nodal, $Nodal^{\Delta ASE/\Delta ASE}$; ΔASE-Nodal-YFP, $Nodal^{\Delta ASE/\Delta ASE-yfp}$; Nodal knockout (KO), $Nodal^{\Delta 23/\Delta 23}$.

(B) Nodal reporter expression in BMP4-stimulated Nodal-YFP EpiLC colonies. (Top) Timeline of BMP4 stimulation. (Lower left) Expression of the fluorescent reporter at t = 23 and 44 h. (Lower right) Averaged (n = 4) radial profiles of fluorescence intensity at regular time intervals. For readability, profiles of day 1 and 2 are presented on separate graphs and SDs are only shown for t = 5 and 44 h.

(C) Same as (B) for WNT3A stimulation.

(D) Effect of an ACTIVIN/NODAL signaling inhibitor (SB) and a WNT secretion inhibitor (IWP2) on Nodal reporter expression in BMP4-stimulated Nodal-YFP EpiLC colonies. Averaged (n = 4) fluorescence intensity profiles.

(E) RT-qPCR quantification of *Lefty2* expression in WT, ΔASE-Nodal and Nodal KO ESCs. Error bars represent the SEM of three independent experiments.

(F) Nodal reporter expression dynamics in Nodal-YFP and ΔASE-Nodal-YFP differentiating EpiLC colonies after WNT3A or BMP4 stimulation. Averaged profiles of n = 4 colonies for each condition. Experiments of (B–D and F) were repeated and gave similar results at least twice. Scale bar, 100μm.

(Papanayotou et al., 2014). This regulatory shift is recapitulated during the conversion of ESCs into EpiLCs.

To investigate how *Nodal* expression levels affect cell-fate specification, we generated homozygous ASE deletions in both WT and *Nodal*$^{+/YFP}$ ESC lines (Figure 3A). We also generated an ESC line homozygous for a loss-of-function mutation of *Nodal*, noted *Nodal*^{Δ23}, by deleting on both alleles a sequence that encodes most of the mature ligand (Figure 3A). *Nodal*$^{ΔASE/ΔASE}$ ESCs expressed the ACTIVIN/NODAL signaling target *Lefty2* at a level comparable with that of WT ESCs (Figure 3E). In contrast, *Lefty2* expression was barely detectable in *Nodal*$^{Δ23/Δ23}$ cells, demonstrating their inability to produce a functional ligand. *Nodal*$^{ΔASE/ΔASE}$ and *Nodal*$^{Δ23/Δ23}$ EpiLCs were obtained in N2B27 + knockout serum replacement (KSR) without AF. They appeared similar to wild-type (WT) EpiLCs (Figures S4A and S4B).

Nodal$^{ΔASE/ΔASE-YFP}$ cells showed a 75% reduction in YFP expression after B or W stimulation, relative to *Nodal*$^{+/YFP}$ cells (Figure 3F). *Nodal*$^{ΔASE/ΔASE-YFP}$ cells nevertheless showed a small increase in YFP expression after stimulation, presumably mediated by the WNT signaling-dependent PEE, because WNT-stimulated cells responded faster than BMP-stimulated ones. The expression of *Nodal* was similarly affected in *Nodal*$^{ΔASE/ΔASE}$ cells, whereas no post-stimulation bumps were detected in *Nodal*$^{Δ23/Δ23}$ cells (Figures S5A and S5B), suggesting that ASE is not the only *Nodal* enhancer mediating the influence of NODAL signaling at this stage.

The 2Dgas thus correctly recapitulate *in vitro* the regulation of *Nodal* expression as it has been characterized in the embryo, and *Nodal*$^{ΔASE/ΔASE}$ and *Nodal*$^{Δ23/Δ23}$ EpiLCs are suitable models to investigate *in vitro* the contribution of *Nodal* to patterning.

Nodal is required to form posterior mesoderm in BMP4-stimulated colonies

We compared the differentiation of WT, *Nodal*$^{ΔASE/ΔASE}$, and *Nodal*$^{Δ23/Δ23}$ EpiLCs in B-stimulated colonies. As before, we performed three independent experiments and analyzed the first with 29 markers; 18 of these were then selected to complete the analysis of all three experiments. The resulting dataset was then used to draw and compare colony differentiation trajectories for each cell line (Figures 4A–4C and S5A).

The analysis of the first experiment grouped the markers into four clusters (Figures 4A and 4B). In the first were early epiblast markers, which tended to be more highly expressed before stimulation. In the second were markers of the maturing epiblast, which normally peaked at t = 0 h and decreased after stimulation. In the third were PS and posterior PS derivatives markers, which were most expressed 48 and 72 h after stimulation in WT colonies. In the fourth cluster were markers associated with a variety

of cell identities, from mature epiblast and non-neural ectoderm to PS and cardiac mesoderm. *Nodal*$^{Δ23/Δ23}$ colonies, like the unstimulated WT colonies above, failed to activate *Bra* expression and showed no evidence of forming a PS and mesoderm derivatives, adopting instead what we identified in cluster 4 as a signature of non-neural ectoderm. This observation supports a strict requirement for *Nodal* in the formation of posterior mesoderm and is consistent with studies that found no sign of mesoderm in *Nodal*$^{-/-}$ embryos (Ben-Haim et al., 2006; Brennan et al., 2001).

The mean developmental trajectories obtained by PCA (Figure 4C) largely confirmed this analysis. They also showed that *Nodal*$^{Δ23/Δ23}$ and *Nodal*$^{ΔASE/ΔASE}$ colonies reached closer endpoints than expected given the dissimilarity of the corresponding embryonic phenotypes (Brennan et al., 2001; Conlon et al., 1994; Norris et al., 2002). This resulted from the fact that *Nodal*$^{ΔASE/ΔASE}$ colonies at the end of the culture had lower expression of PS markers and higher expression of ectodermal markers than WT colonies. Although they expressed *Bra* and other PS and posterior mesoderm markers, most peaked at 48 h and declined afterward (Figures 4C and S5A–S5C). Expression of cluster 4 genes *Tp63*, *Pax3*, *Tfap2a*, and *Id1* was also closer to that observed in *Nodal*$^{Δ23/Δ23}$ colonies than in WT colonies. Immunostaining confirmed the differentiation of *Nodal*$^{ΔASE/ΔASE}$ colonies toward an ectodermal identity as they expressed TFAP2A homogeneously, as *Nodal*$^{Δ23/Δ23}$ colonies did. Most *Nodal*$^{ΔASE/ΔASE}$ colonies also expressed BRA, GATA6, and CDX2 in irregular patches of varying size and number, but the proportion of cells expressing these markers was drastically reduced at the end of the culture (Figures 4D–4F and S5C).

These results demonstrate a strict requirement for *Nodal* to form the PS and posterior PS derivatives. They also reveal that the patterning of m2Dgas is more sensitive to *Nodal* expression levels than that of the epiblast, because no gastrulation defects were reported in *Nodal*$^{ΔASE/ΔASE}$ embryos (Norris et al., 2002).

Low *Nodal* expression is sufficient to specify anterior PS derivatives

We then compared the differentiation of colonies from the same three cell lines after W stimulation. The gene expression dynamics of the markers used in a first experiment identified three clusters (Figures 5A and 5B): the first contained markers of early and maturing epiblast; the second, markers for the anterior ectoderm and the neurectoderm; and the third, markers of the PS and its derivatives. As before, W stimulation promoted the emergence of epiblast and PS derivatives of anterior character in WT colonies. In *Nodal*$^{Δ23/Δ23}$ colonies, anterior ectodermal and neural markers were more strongly induced, while expression
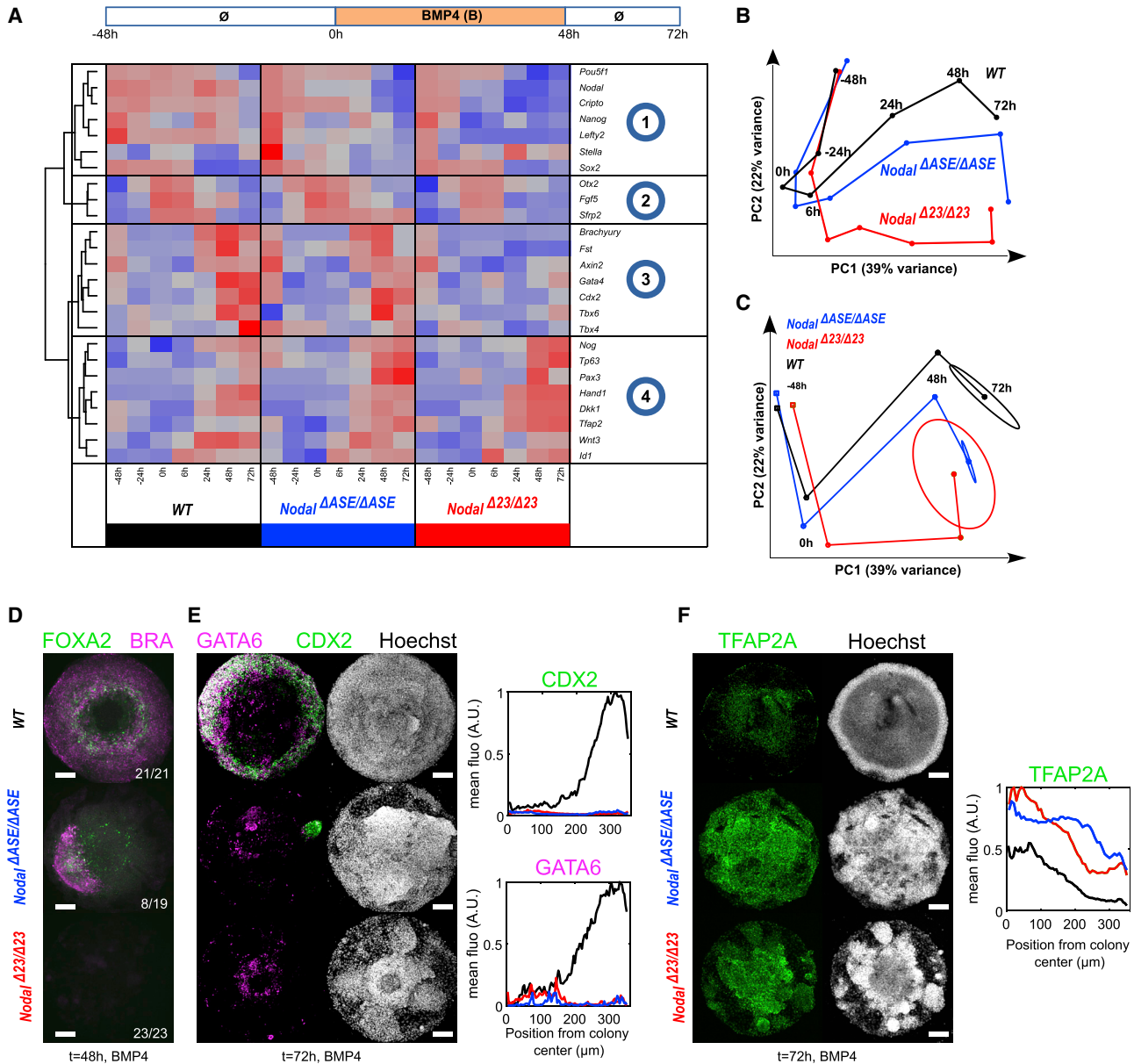
Figure 4. _Nodal_ is required to form posterior mesoderm in m2Dgas

(A) (Top) Timeline of BMP4 stimulation. (Bottom) Gene expression matrix obtained via RT-qPCR of pooled colonies at similar time points for the WT, ΔASE-Nodal, and Nodal KO cell lines. Expression dynamics comparison led to the grouping of markers into four distinct clusters.

(B) Projection of the RT-qPCR data shown in (A) in the space defined by the first two principal components of the dataset shows the developmental trajectories of WT and mutant colonies.

(C) Average developmental trajectories obtained from three independent experiments using a selection of 18 markers. The overlap of the 95% confidence ellipses at two endpoints indicates some similarity.

(D) Maximum intensity projections (MIPs) of representative WT and _Nodal_ mutant colonies immunostained 48 h after the start of BMP4 stimulation.

(E and F) MIPs of representative WT and _Nodal_ mutant colonies immunostained 72 h after the start of BMP4 stimulation and corresponding average (n = 4) radial profiles. Experiments of (D–F) were repeated and gave similar results at least twice. Scale bar 100 μm. See Figure S4 for additional examples of the patterns obtained for ΔASE-Nodal colonies.
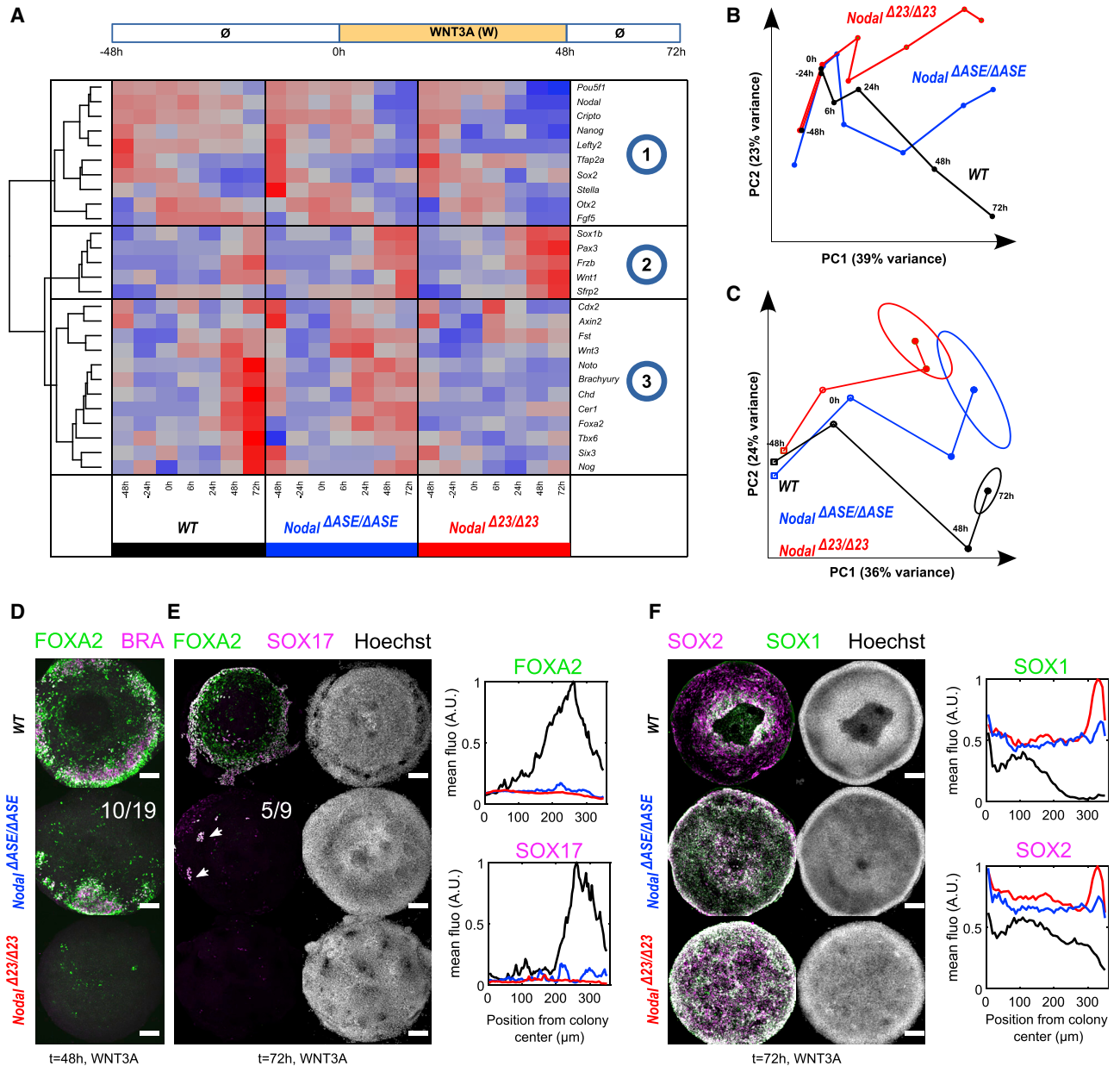
Figure 5. Low *Nodal* expression does not prevent the emergence of anterior PS identities

(A) (Top) Timeline of WNT3A stimulation. (Bottom) Gene expression matrix obtained via RT-qPCR of pooled colonies at similar time points for the WT, ΔASE-Nodal, and Nodal KO cell lines. Expression dynamics comparison led to the grouping of markers into three distinct clusters.

(B) Projection of the RT-qPCR data shown in (A) in the space defined by the first two principal components of the dataset shows the developmental trajectories of WT and mutant colonies.

(C) Average developmental trajectories obtained from three independent experiments using a selection of 18 markers. The overlap of the 95% confidence ellipses at two endpoints indicates some similarity.

(D) Maximum intensity projections (MIPs) of representative WT and *Nodal* mutant colonies immunostained 48 h after the start of WNT3A stimulation.

(E and F) MIPs of representative WT and *Nodal* mutant colonies immunostained 72 h after the start of WNT3A stimulation and corresponding average (n = 4) radial profiles. Experiments of (D–F) were repeated and gave similar results at least twice. Scale bar 100 μm. See Figure S4 for additional examples of the patterns obtained for ΔASE-Nodal colonies.

of most PS and PS derivative markers remained at very low levels. A notable exception was *Cdx2*, which was transiently activated shortly after stimulation. *Nodal*$^{ΔASE/ΔASE}$ colonies again showed a stronger phenotype than expected, activating the expression of ectodermal and neural markers to levels similar to those of *Nodal*$^{Δ23/Δ23}$ colonies. Although they expressed PS and anterior PS derivatives markers (such as *Bra*, *Noto*, *Cer1*, and *Foxa2*), they did not reach the levels seen in WT colonies.

The 18 markers were selected to analyze three independent experiments (Figure S5A). PCA of the resulting dataset allowed us to plot mean developmental trajectories (Figure 5C). While that of the *Nodal*$^{ΔASE/ΔASE}$ colonies was initially close to that of the WT colonies, its endpoint was closer to that of *Nodal*$^{Δ23/Δ23}$ colonies (Figure 5C). The similarity between *Nodal*$^{ΔASE/ΔASE}$ colonies and *Nodal*$^{Δ23/Δ23}$ colonies was confirmed by immunostaining, showing that SOX1 and SOX2 were expressed from the center to the edge in both types of colonies (Figures 5D–5F). However, W-stimulated *Nodal*$^{ΔASE/ΔASE}$ colonies displayed similar patches of BRA or FOXA2 expression as B-stimulated *Nodal*$^{ΔASE/ΔASE}$ colonies, with the same variability in size and expression levels (Figures 4D, 5D, and S5C), except that this time FOXA2 was clearly co-expressed with BRA, as befits anterior PS derivatives (Figure 5D). This, and the detection of small clusters of DE cells co-expressing FOXA2 and SOX17 in some colonies after 72 h culture (Figure 5E), suggest that the drastic decrease in *Nodal* expression resulted in a reduction of the number of anterior mesendoderm cells but not in their replacement by cells of a more posterior PS identity.

These results show that the formation of anterior PS derivatives can be obtained in a context where *Nodal* is expressed at low level. Their maintenance, as well as the robustness and reproducibility of colony patterning, are, however, critically dependent on the ASE enhancer.

DISCUSSION

We exposed micropatterned EpiLC colonies to different morphogens to model mouse gastrulation *in vitro*. Although the protocol we used was slightly different from that described in another report (Morgani et al., 2018), we obtained similar differentiation patterns, attesting to the robustness of the approach.

The fact that *Nodal*$^{−/−}$ EpiLC colonies failed to express markers of the PS and its derivatives when stimulated with BMP4 or WNT3A underlines a strict requirement for *Nodal* for both PS formation and the specification of mesendodermal identities. This is in agreement with embryological studies that found no evidence of expression of PS or nascent mesoderm markers in *Nodal*$^{−/−}$ embryos (Ben-Haim et al., 2006; Brennan et al., 2001) and finally demonstrates that neither BMP4 nor WNT3A can compensate for NODAL absence. The fact that *Nodal*$^{−/−}$ colonies form ectodermal and neural cell identities is also consistent with their premature emergence in *Nodal*$^{−/−}$ embryos (Camus et al., 2006). These results position Nodal as the determining factor in a binary choice between ectodermal and mesendodermal identities. They are consistent with Nodal acting upstream of the TBX factors Eomes and BRA, which have recently been shown to govern the same binary choice via their impact on chromatin state (Tosic et al., 2019).

Our results, in line with previous reports (Faial et al., 2015; Morgani et al., 2018), strongly suggest that BMP4, in addition to promoting posterior PS cell fates, actively suppresses anterior ones. This is consistent with anterior PS identities emerging from a region of the embryo that is initially beyond the reach of diffusing BMP4 molecules and later sees local activation of the expression of BMP antagonists (Bachiller et al., 2000; Zhang et al., 2019). There are several examples of BMP signaling antagonizing ACTIVIN/NODAL/Nodal signaling during embryogenesis (Furtado et al., 2008; Pereira et al., 2012; Yamamoto et al., 2009). These situations involve a component common to both pathways being limiting and competition for it favoring BMP signaling. The situation is, however, different in micropatterned colonies, and presumably in the PS, because the WNT and ACTIVIN/NODAL signaling pathways were still active in BMP4-stimulated colonies, possibly even more so given the increase in the expression of their respective feedback antagonists *Axin2* and *Lefty2*. Although this should dampen WNT and NODAL signaling, it also suggests the possibility of a selective impact of BMP signaling on the expression of some of their targets. Furthermore, BMP4-stimulated *Nodal*$^{ΔASE/ΔASE}$ EpiLC colonies, where *Nodal* expression is drastically reduced, failed to maintain the posterior PS derivatives they formed initially, indicating that maintaining a higher level of *Nodal* expression is required to do so, in addition to its prior requirement for PS formation. These observations suggest that, although BMP4 prevents Nodal and WNT3a from activating the anterior PS developmental program, it does not block their signaling pathways but rather recruits them to assist in promoting posterior PS development.

The fact that *Nodal*$^{ΔASE/ΔASE}$ EpiLC colonies were unable to form radial differentiation patterns is evidence that the ability of cells to respond to and reflect local Nodal exposure is essential for patterning. The random patches of mesoderm that formed on some colonies may, however, suggest that the remaining active *Nodal* enhancers, HBE and PEE, sometimes manage to initiate a small autoregulatory response. This is consistent with reports that ACTIVIN/NODAL signaling is part of the regulatory input of these enhancers (Funa et al., 2015; Papanayotou et al.,

2014) and with the small bump of *Nodal* expression detected in these colonies 24 h after stimulation. With its activation taking place after stimulation, a limited PEE-driven auto-inductive response could explain the formation of unstable patches of BRA-positive cells. The fact that a similar phenotype was not seen in *Nodal*$^{\Delta ASE/\Delta ASE}$ embryos strongly suggests that Nodal depletion was compensated by ligands of extra-embryonic or maternal origin in these embryos (Norris et al., 2002). Two other transforming growth factor β (TGF-β) family members present at these stages are GDF1 and GDF3, but neither of them appears capable of compensating for Nodal absence (Andersson et al., 2007; Granier et al., 2011; Levine et al., 2009). Furthermore, we found that both types of *Nodal* mutant colonies developed their drastic phenotypes despite maintaining WT levels of *Gdf3* expression. A better candidate may be the ACTIVIN produced by extra-embryonic and decidual cells (Albano et al., 1994; Pijuan-Sala et al., 2019).

The PS derivatives that formed on *Nodal*$^{\Delta ASE/\Delta ASE}$ colonies within 48 h had identities that matched the stimulation, posterior for BMP4 and anterior for WNT3A, despite *Nodal* expression remaining well below its normal levels. However, their maintenance was found to depend in both conditions on sustained higher *Nodal* expression as their cell numbers had dwindled by the end of the culture. This does not seem to fit models where differences in the level or duration of Nodal signaling are what leads to the specification of distinct PS cell identities. These observations suggest instead a two-step process where emerging cell identities initially reflect the combination of signals their progenitors were exposed to, whereas their expansion depends on Nodal signaling reaching certain levels. Interestingly, the list of transcription factors partnering with SMAD2/3 and known to play a role in PS patterning has expanded in recent years. It now includes, in addition to SMAD4 and FOXH1 (Chu et al., 2004; Hoodless et al., 2001; Yamamoto et al., 2001), transcription factors, such as OCT4, NANOG, Eomes, and BRA, some of which are also SMAD1 partners (Faial et al., 2015; Mulas et al., 2017; Mullen et al., 2011; Suzuki et al., 2006). This mix of effectors, and the potential for both competition and cooperation it implies, appears permissive to PS cell-fate specification involving some combinatorial process. Further investigations will be necessary to determine whether this is actually the case.

We noticed that below a certain cell density, mouse colonies do not get patterned whereas human ones do. The patterning of h2Dgas was shown to be critically dependent on BMP signaling being restricted to the edge of colonies. This results from TGF-β receptors remaining accessible to apically applied ligands at the edge of colonies, but not at their center, and from the expression of the BMP antagonist NOGGIN (Etoc et al., 2016). However, *Noggin*$^{-/-}$ mouse embryos display no gastrulation phenotype (McMahon et al., 1998). This is consistent with the comparatively late onset of *Noggin* expression during mouse development and in our m2Dgas and the fact that, unlike in hESCs, it is not directly induced by BMP4 in EpiSCs (Etoc et al., 2016). The early absence of this antagonist could be what makes m2Dgas patterning more reliant on cell density and epithelialization to restrict BMP signaling to the edge of colonies. It could also explain why *Nodal* expression is first induced in the entire colony before being restricted at the edge of m2DGas, while it moves inward from the colony edge in h2DGas (Chhabra et al., 2019). Differences between mouse and human colonies in how their patterning unfolds may thus reflect actual differences in how gastrulation proceeds in the two species.

To summarize, the patterning of m2Dgas is largely consistent with the embryological data. The discrepancies we identified highlighted gaps in our understanding of the mechanisms underlying the patterning of the PS. The m2DGas model system is, therefore, complementary to embryological studies and will address unresolved issues of gastrulation *in vitro*.

EXPERIMENTAL PROCEDURES

Cell culture and cell lines

All ESC lines used are HM1 (Selfridge et al., 1992), except the Nodal-YFP and ΔASE-Nodal-YFP lines, which are CK35 (Papanayotou et al., 2014). ESCs were cultured on 0.15% gelatin-coated plates in N2B27 medium supplemented with MAPK/ERK pathway and glycogen synthase kinase 3 (GSK3) inhibitors and leukemia inhibitory factor (2i+LIF) (Silva et al., 2008). The *Nodal*$^{-/-}$ and *Nodal*$^{\Delta ASE/\Delta ASE}$ lines were generated via CRISPR/Cas9 editing. A 1196 bp deletion spanning exons two and three prevents Nodal production in the *Nodal*$^{-/-}$ line. The *Nodal*$^{\Delta ASE/\Delta ASE}$ line contains a 600 bp ASE deletion similar to that previously described (Norris et al., 2002).

EpiLCs differentiation on micropatterned adhesive substrates

ESCs were seeded on fibronectin-coated (15 μg/mL for 30 min) plates and cultured in N2B27 + 1% KSR, optionally supplemented with 20 ng/mL ACTIVIN and 12 ng/mL FGF2. After 24 h, cells were trypsinized and seeded at a density of 8,000 cells/mm^2 on micropatterned substrates produced by microcontact printing of fibronectin on polydimethylsiloxane (PDMS)-coated glass coverslips. After 1 h, unattached cells were removed. Colonies were cultured for an additional 24 h before stimulation began (BMP4: 50 ng/mL, WNT3A: 200 ng/mL, AACTIVIN: 20 ng/mL, and FGF2: 12 ng/mL). The medium was renewed every 24 h. See supplemental information and Simon et al., 2022 for detailed protocols.

Quantitative analysis of gene expression

Standard RT-qPCR was used to quantify gene expression. A custom R script was used to compute the following steps. Markers expressed at

low level—with a difference of at least 10 between their cycle quantification (Cq) value and that of glyceraldehyde-3 phosphate dehydrogenase (GAPDH)—were removed from the analysis in all samples considered. For each marker in each sample, a relative gene expression value was computed with respect to the mean expression of the gene in the experiment (pooling all samples) and normalized by the expression of GAPDH in the sample. This value was log2-transformed and then centered and reduced with respect to the expression value of the gene in all samples considered in order to compute and display the expression matrix and the PCA of this matrix.

See supplemental information for a complete list of reagents, primers, and antibodies used.

SUPPLEMENTAL INFORMATION

Supplemental information can be found online at https://doi.org/10.1016/j.stemcr.2022.05.009.

CONFLICTS OF INTEREST

The authors declare no conflict of interest.

REFERENCES

Albano, R.M., Arkell, R., Beddington, R.S.P., and Smith, J.C. (1994). Expression of inhibin subunits and follistatin during postimplantation mouse development: decidual expression of activin and expression of follistatin in primitive streak, somites and hindbrain. Development 120, 803–813.

Andersson, O., Bertolino, P., and Ibáñez, C.F. (2007). Distinct and cooperative roles of mammalian Vg1 homologs GDF1 and GDF3 during early embryonic development. Dev. Biol. 311, 500–511. https://doi.org/10.1016/j.ydbio.2007.08.060.

Bachiller, D., Klingensmith, J., Kemp, C., Belo, J.A., Anderson, R.M., May, S.R., McMahon, J.A., McMahon, A.P., Harland, R.M., Rossant, J., et al. (2000). The organizer factors Chordin and Noggin are required for mouse forebrain development. Nature 403, 658–661. https://doi.org/10.1038/35001072.

Ben-Haim, N., Lu, C., Guzman-Ayala, M., Pescatore, L., Mesnard, D., Bischofberger, M., Naef, F., Robertson, E.J., and Constam, D.B. (2006). The nodal precursor acting via activin receptors induces mesoderm by maintaining a source of its convertases and BMP4. Dev. Cell 11, 313–323. https://doi.org/10.1016/j.devcel.2006.07.005.

Brennan, J., Lu, C.C., Norris, D.P., Rodriguez, T.A., Beddington, R.S.P., and Robertson, E.J. (2001). Nodal signalling in the epiblast patterns the early mouse embryo. Nature 411, 965–969. https://doi.org/10.1038/35082103.

Buecker, C., Srinivasan, R., Wu, Z., Calo, E., Acampora, D., Faial, T., Simeone, A., Tan, M., Swigut, T., and Wysocka, J. (2014). Reorganization of enhancer patterns in transition from naive to primed pluripotency. Cell Stem Cell 14, 838–853. https://doi.org/10.1016/j.stem.2014.04.003.

Burtscher, I., and Lickert, H. (2009). Foxa2 regulates polarity and epithelialization in the endoderm germ layer of the mouse embryo. Development 136, 1029–1038. https://doi.org/10.1242/dev.028415.

Camacho-Aguilar, E., and Warmflash, A. (2020). Insights into mammalian morphogen dynamics from embryonic stem cell systems. In Current Topics in Developmental Biology (Elsevier), pp. 279–305.

Camus, A., Perea-Gomez, A., Moreau, A., and Collignon, J. (2006). Absence of Nodal signaling promotes precocious neural differentiation in the mouse embryo. Dev. Biol. 295, 743–755. https://doi.org/10.1016/j.ydbio.2006.03.047.

Chhabra, S., Liu, L., Goh, R., Kong, X., and Warmflash, A. (2019). Dissecting the dynamics of signaling events in the BMP, WNT, and NODAL cascade during self-organized fate patterning in human gastruloids. PLoS Biol. 17, e3000498. https://doi.org/10.1371/journal.pbio.3000498.

Chu, G.C., Dunn, N.R., Anderson, D.C., Oxburgh, L., and Robertson, E.J. (2004). Differential requirements for Smad4 in TGFbeta-dependent patterning of the early mouse embryo. Development 131, 3501–3512. https://doi.org/10.1242/dev.01248.

Collignon, J., Varlet, I., and Robertson, E.J. (1996). Relationship between asymmetric nodal expression and the direction of embryonic turning. Nature 381, 155–158. https://doi.org/10.1038/381155a0.

Conlon, F.L., Lyons, K.M., Takaesu, N., Barth, K.S., Kispert, A., Herrmann, B., and Robertson, E.J. (1994). A primary requirement for nodal in the formation and maintenance of the primitive streak in the mouse. Development 120, 1919–1928.

Deglincerti, A., Etoc, F., Guerra, M.C., Martyn, I., Metzger, J., Ruzo, A., Simunovic, M., Yoney, A., Brivanlou, A.H., Siggia, E., and Warmflash, A. (2016). Self-organization of human embryonic

stem cells on micropatterns. Nat. Protoc. *11*, 2223–2232. https://doi.org/10.1038/nprot.2016.131.

Du, P., Pirouz, M., Choi, J., Huebner, A.J., Clement, K., Meissner, A., Hochedlinger, K., and Gregory, R.I. (2018). An intermediate pluripotent state controlled by MicroRNAs is required for the naive-to-primed stem cell transition. Cell Stem Cell *22*, 851–864. https://doi.org/10.1016/j.stem.2018.04.021.

Etoc, F., Metzger, J., Ruzo, A., Kirst, C., Yoney, A., Ozair, M.Z., Brivanlou, A.H., and Siggia, E.D. (2016). A balance between secreted inhibitors and edge sensing controls gastruloid self-organization. Dev. Cell *39*, 302–315. https://doi.org/10.1016/j.devcel.2016.09.016.

Faial, T., Bernardo, A.S., Mendjan, S., Diamanti, E., Ortmann, D., Gentsch, G.E., Mascetti, V.L., Trotter, M.W.B., Smith, J.C., and Pedersen, R.A. (2015). Brachyury and SMAD signalling collaboratively orchestrate distinct mesoderm and endoderm gene regulatory networks in differentiating human embryonic stem cells. Development *142*, 2121–2135. https://doi.org/10.1242/dev.117838.

Funa, N.S., Schachter, K.A., Lerdrup, M., Ekberg, J., Hess, K., Dietrich, N., Honoré, C., Hansen, K., and Semb, H. (2015). β-Catenin regulates primitive streak induction through collaborative interactions with SMAD2/SMAD3 and OCT4. Cell Stem Cell *16*, 639–652. https://doi.org/10.1016/j.stem.2015.03.008.

Furtado, M.B., Solloway, M.J., Jones, V.J., Costa, M.W., Biben, C., Wolstein, O., Preis, J.I., Sparrow, D.B., Saga, Y., Dunwoodie, S.L., et al. (2008). BMP/SMAD1 signaling sets a threshold for the left/right pathway in lateral plate mesoderm and limits availability of SMAD4. Genes Dev. *22*, 3037–3049. https://doi.org/10.1101/gad.1682108.

Granier, C., Gurchenkov, V., Perea-Gomez, A., Camus, A., Ott, S., Papanayotou, C., Iranzo, J., Moreau, A., Reid, J., Koentges, G., et al. (2011). Nodal cis-regulatory elements reveal epiblast and primitive endoderm heterogeneity in the peri-implantation mouse embryo. Dev. Biol. *349*, 350–362. https://doi.org/10.1016/j.ydbio.2010.10.036.

Harland, R.M. (1994). Commentary the transforming growth factor , family and induction of the vertebrate mesoderm: bone morphogenetic proteins are ventral inducers. Proc. Natl. Acad. Sci. U S A *4*, 10243–10246.

Hayashi, K., Ohta, H., Kurimoto, K., Aramaki, S., and Saitou, M. (2011). Reconstitution of the mouse germ cell specification pathway in culture by pluripotent stem cells. Cell *146*, 519–532. https://doi.org/10.1016/j.cell.2011.06.052.

Hoodless, P.A., Pye, M., Chazaud, C., Labbé, E., Attisano, L., Rossant, J., and Wrana, J.L. (2001). FoxH1 (Fast) functions to specify the anterior primitive streak in the mouse. Genes Dev. *15*, 1257–1271. https://doi.org/10.1101/gad.881501.

Kinder, S.J., Tsang, T.E., Quinlan, G.A., Hadjantonakis, A.K., Nagy, A., and Tam, P.P. (1999). The orderly allocation of mesodermal cells to the extraembryonic structures and the anteroposterior axis during gastrulation of the mouse embryo. Development *126*, 4691–4701.

Kinoshita, M., Barber, M., Mansfield, W., Cui, Y., Spindlow, D., Stirparo, G.G., Dietmann, S., Nichols, J., and Smith, A. (2021). Capture of mouse and human stem cells with features of formative pluripotency. Cell Stem Cell *28*, 453–471.e8. https://doi.org/10.1016/j.stem.2020.11.005.

Levine, A.J., Levine, Z.J., and Brivanlou, A.H. (2009). GDF3 is a BMP inhibitor that can activate Nodal signaling only at very high doses. Dev. Biol. *325*, 43–48. https://doi.org/10.1016/j.ydbio.2008.09.006.

Liu, P., Wakamiya, M., Shea, M.J., Albrecht, U., Behringer, R.R., and Bradley, A. (1999). Requirement for Wnt3 in vertebrate axis formation. Nat. Genet. *22*, 361–365. https://doi.org/10.1038/11932.

Martyn, I., Siggia, E.D., and Brivanlou, A.H. (2019). Mapping cell migrations and fates in a gastruloid model to the human primitive streak. Development *146*, dev179564.

McMahon, J.A., Takada, S., Zimmerman, L.B., Fan, C.-M., Harland, R.M., and McMahon, A.P. (1998). Noggin-mediated antagonism of BMP signaling is required for growth and patterning of the neural tube and somite. Genes Dev. *12*, 1438–1452. https://doi.org/10.1101/gad.12.10.1438.

Morgani, S.M., and Hadjantonakis, A.-K. (2020). Signaling regulation during gastrulation: insights from mouse embryos and in vitro systems. In Current Topics in Developmental Biology (Elsevier), pp. 391–431.

Morgani, S.M., and Hadjantonakis, A.-K. (2021). Spatially organized differentiation of mouse pluripotent stem on micropatterned surfaces. In Epigenetic Reprogramming During Mouse Embryogenesis, K. Ancelin and M. Borensztein, eds. (Springer US)), pp. 41–58.

Morgani, S.M., Metzger, J.J., Nichols, J., Siggia, E.D., and Hadjantonakis, A.-K. (2018). Micropattern differentiation of mouse pluripotent stem cells recapitulates embryo regionalized cell fate patterning. Elife *7*, e32839. https://doi.org/10.7554/eLife.32839.

Mulas, C., Kalkan, T., and Smith, A. (2017). NODAL secures pluripotency upon embryonic stem cell progression from the ground state. Stem Cell Rep. *9*, 77–91. https://doi.org/10.1016/j.stemcr.2017.05.033.

Mullen, A.C., Orlando, D.A., Newman, J.J., Lovén, J., Kumar, R.M., Bilodeau, S., Reddy, J., Guenther, M.G., DeKoter, R.P., and Young, R.A. (2011). Master transcription factors determine cell-type-specific responses to TGF-β signaling. Cell *147*, 565–576. https://doi.org/10.1016/j.cell.2011.08.050.

Norris, D.P., Brennan, J., Bikoff, E.K., and Robertson, E.J. (2002). The Foxh1-dependent autoregulatory enhancer controls the level of Nodal signals in the mouse embryo. Development *129*, 3455–3468.

Osorno, R., Tsakiridis, A., Wong, F., Cambray, N., Economou, C., Wilkie, R., Blin, G., Scotting, P.J., Chambers, I., and Wilson, V. (2012). The developmental dismantling of pluripotency is reversed by ectopic Oct4 expression. Development *139*, 2288–2298. https://doi.org/10.1242/dev.078071.

Papanayotou, C., Benhaddou, A., Camus, A., Perea-Gomez, A., Jouneau, A., Mezger, V., Langa, F., Ott, S., Sabéran-Djoneidi, D., and Collignon, J. (2014). A novel nodal enhancer dependent on pluripotency factors and smad2/3 signaling conditions a regulatory switch during epiblast maturation. PLoS Biol. *12*, e1001890. https://doi.org/10.1371/journal.pbio.1001890.

Peng, G., Suo, S., Chen, J., Chen, W., Liu, C., Yu, F., Wang, R., Chen, S., Sun, N., Cui, G., et al. (2016). Spatial transcriptome for the molecular annotation of lineage fates and cell identity in mid-gastrula mouse embryo. Dev. Cell 36, 681–697. https://doi.org/10.1016/j.devcel.2016.02.020.

Perea-Gomez, A., Camus, A., Moreau, A., Grieve, K., Moneron, G., Dubois, A., Cibert, C., and Collignon, J. (2004). Initiation of gastrulation in the mouse embryo is preceded by an apparent shift in the orientation of the anterior-posterior Axis. Curr. Biol. 14, 197–207. https://doi.org/10.1016/j.cub.2004.01.030.

Pereira, P.N.G., Dobreva, M.P., Maas, E., Cornelis, F.M., Moya, I.M., Umans, L., Verfaillie, C.M., Camus, A., de Sousa Lopes, S.M.C., Huylebroeck, D., et al. (2012). Antagonism of Nodal signaling by BMP/Smad5 prevents ectopic primitive streak formation in the mouse amnion. Development 139, 3343–3354. https://doi.org/10.1242/dev.075465.

Pijuan-Sala, B., Griffiths, J.A., Guibentif, C., Hiscock, T.W., Jawaid, W., Calero-Nieto, F.J., Mulas, C., Ibarra-Soria, X., Tyser, R.C.V., Ho, D.L.L., et al. (2019). A single-cell molecular map of mouse gastrulation and early organogenesis. Nature 566, 490–495. https://doi.org/10.1038/s41586-019-0933-9.

Rivera-Pérez, J.A., and Magnuson, T. (2005). Primitive streak formation in mice is preceded by localized activation of Brachyury and Wnt3. Dev. Biol. 288, 363–371. https://doi.org/10.1016/j.ydbio.2005.09.012.

Selfridge, J., Pow, A.M., McWhir, J., Magin, T.M., and Melton, D.W. (1992). Gene targeting using a mouse HPRT minigene/HPRT-deficient embryonic stem cell system: inactivation of the mouse ERCC-1 gene. Somat. Cell Mol. Genet. 18, 325–336. https://doi.org/10.1007/BF01235756.

Silva, J., Barrandon, O., Nichols, J., Kawaguchi, J., Theunissen, T.W., and Smith, A. (2008). Promotion of reprogramming to ground state pluripotency by signal inhibition. PLoS Biol. 6, e253. https://doi.org/10.1371/journal.pbio.0060253.

Simon, G., Plouhinec, J.-L., and Sorre, B. (2022). Differentiation of EpiLCs on micropatterned substrates generated by micro-contact printing. In Epiblast Stem Cells - Methods and Protocols, Pierre Osteil, ed. (Springer US).

Suzuki, A., Raya, Á., Kawakami, Y., Morita, M., Matsui, T., Nakashima, K., Gage, F.H., Rodríguez-Esteban, C., and Izpisúa Belmonte, J.C. (2006). Nanog binds to Smad1 and blocks bone morphogenetic protein-induced differentiation of embryonic stem cells. Proc. Natl. Acad. Sci. U S A 103, 10294–10299. https://doi.org/10.1073/pnas.0506945103.

Tosic, J., Kim, G.-J., Pavlovic, M., Schröder, C.M., Mersiowsky, S.-L., Barg, M., Hofherr, A., Probst, S., Köttgen, M., Hein, L., et al. (2019). Eomes and Brachyury control pluripotency exit and germ-layer segregation by changing the chromatin state. Nat. Cell Biol. 21, 1518–1531. https://doi.org/10.1038/s41556-019-0423-1.

Vincent, S.D., Dunn, N.R., Hayashi, S., Norris, D.P., and Robertson, E.J. (2003). Cell fate decisions within the mouse organizer are governed by graded Nodal signals. Genes Dev. 17, 1646–1662. https://doi.org/10.1101/gad.1100503.

Warmflash, A., Sorre, B., Etoc, F., Siggia, E.D., and Brivanlou, A.H. (2014). A method to recapitulate early embryonic spatial patterning in human embryonic stem cells. Nat. Methods 11, 847–854. https://doi.org/10.1038/nmeth.3016.

Winnier, G., Blessing, M., Labosky, P.A., and Hogan, B.L. (1995). Bone morphogenetic protein-4 is required for mesoderm formation and patterning in the mouse. Genes Dev. 9, 2105–2116. https://doi.org/10.1101/gad.9.17.2105.

Yamamoto, M., Meno, C., Sakai, Y., Shiratori, H., Mochida, K., Ikawa, Y., Saijoh, Y., and Hamada, H. (2001). The transcription factor FoxH1 (FAST) mediates Nodal signaling during anterior-posterior patterning and node formation in the mouse. Genes Dev. 15, 1242–1256. https://doi.org/10.1101/gad.883901.

Yamamoto, M., Beppu, H., Takaoka, K., Meno, C., Li, E., Miyazono, K., and Hamada, H. (2009). Antagonism between Smad1 and Smad2 signaling determines the site of distal visceral endoderm formation in the mouse embryo. J. Cell Biol. 184, 323–334. https://doi.org/10.1083/jcb.200808044.

Zhang, Z., Zwick, S., Loew, E., Grimley, J.S., and Ramanathan, S. (2019). Mouse embryo geometry drives formation of robust signaling gradients through receptor localization. Nat. Commun. 10, 4516. https://doi.org/10.1038/s41467-019-12533-7.

Zhou, X., Sasaki, H., Lowe, L., Hogan, B.L.M., and Kuehn, M.R. (1993). Nodal is a novel TGF-β-like gene expressed in the mouse node during gastrulation. Nature 361, 543–547. https://doi.org/10.1038/361543a0.

Zorn, A.M., Butler, K., and Gurdon, J.B. (1999). Anterior endomesoderm specification in Xenopus by Wnt/beta-catenin and TGF-beta signalling pathways. Dev. Biol. 16, 282–297.